Bacterial strategies in prolonged stationary phase: Tradeoff between cell growth, maintenance, and recycling

Qing Zhang [1,2,*] Yining Chen [1,3] and Hualin Shi [1,3,4,†]

[1] *CAS Key Laboratory of Theoretical Physics, Institute of Theoretical Physics, Chinese Academy of Sciences, Beijing 100190, China*

[2] *CAS Key Laboratory of Genome Sciences and Information, Beijing Institute of Genomics, Chinese Academy of Sciences, and China National Center for Bioinformation, Beijing 100101, China*

[3] *School of Physical Sciences, University of Chinese Academy of Sciences, Beijing 100049, China*

[4] *Wenzhou Institute, University of Chinese Academy of Sciences, Zhejiang 325000, China*

(Received 15 December 2022; accepted 30 January 2023; published 16 February 2023)

In continuous starvation, bacteria will enter an extended stationary phase after the death phase. Growth-advantaged genetic mutations gradually emerge in the long-term stationary phase. The different competition patterns between younger and aged cultures, and the constant density and heterogeneity of living cells in very-aged cultures indicate the complexity of population dynamics under prolonged starvation. Based on resource conservation and protein allocation, here we constructed a simple growth-death-recycling model to describe the population dynamics of one or two bacterial strains during long-term starvation. Through analytical derivation or numerical simulation, we produced the survival-extinction phase diagram of one strain at steady state, and that of two strains at steady state, in a limited detection time, or consuming different nutrients. By relating allocated proteomic fractions to growth, death, and recycling rates, we showed the effects of proteome allocation on the phase diagrams. The constraints and optimization of protein allocation lead to the tradeoff between processes for cell growth, maintenance (repair), and nutrient recycling. The results reveal multiple strategies of bacterial survival and coexistence during long-term starvation.

DOI: 10.1103/PhysRevResearch.5.013119

I. INTRODUCTION

Bacteria need to consume nutrients for continuous growth and proliferation. However, unlike in the laboratory, the bacteria do not easily obtain continuous rich nutrients from the natural environment, and may even endure long-term starvation. The dynamics of the bacterial population is influenced by qualities and levels of environmental nutrients. The fluctuation of nutrient availability in the bacterial life has been described by a prevalent "feast-famine" model [1]. In the long-term batch incubation, bacterial population growth undergo several classical phases: Lag, exponential, stationary, death, and long-term stationary phases [1–3]. When the bacteria grow in the exponential phase, it is easy to do steady-state analyses and define an exponential growth rate; the growth rate dependence of parameters related to cell composition, macromolecules' synthesis, or gene expression has been well characterized [4,5]. Most of nutrients in the culture will be consumed at the exponential phase. When nutrients are nearly exhausted, stringent response signals (e.g., ppGpp and σ_S) will be produced to limit and eventually stop the growth of cells and trigger the transition from the exponential growth to the stationary phase of 2-3 days [1–3]. The further incubation of batch culture after the stationary phase will lead to continuous death (even extinction) of the bacteria (i.e., the death phase) [1–3]. Recent evidence showed that the death rate caused by nutrient deprivation depends on the initial density of viable cells [6] and pregrowth conditions [7].

In the laboratory, a prolonged stationary phase following the death phase has been observed when the bacteria were continuously incubated in a container without nutrient supplementation [1,6,8,9]. In the prolonged stationary phase, a low density of surviving bacterial population can last for months and even years [1,8,10]. Competition experiments of "young" and "aged" cultures or different "aged" cultures demonstrated that mutations resulting in the phenotype of growth advantage in stationary phase (GASP) can emerge in the long-term (e.g., 10 days) incubation [11,12]. The GASP mutant emerged in the older culture can gradually take over the population along with the death of cells from younger cultures and the consecutive emergence of GASP mutants lead to the dynamic alternation of GASP populations [1,10,12]. GASP mutations have been identified in some global genes, e.g., alternative sigma factor gene *rpoS* and transcription factor gene *lrp* [1,10,13] and specific stress genes, e.g., cold shock genes *cspB* and *cspl* [9].

The coexistence of multiple bacterial mutants has been observed in the seasonal [14] or space-heterogeneous nutrient environment [15]. This reflects alternate or separated growth advantages of coexisting mutants with the change in the time or space. The diversity of bacterial population

*zhangq@big.ac.cn
†shihl@itp.ac.cn

in long-term starvation cultures suggests different GASP mutants coexist in a spatiotemporal homogeneous environment [1,3,10,12]. There are fewer studies of the coexistence of different bacterial mutants in spatially and temporally homogeneous environments compared with heterogeneous environments. The conditions under which bacteria coexist in a homogeneous environment may differ from those in a heterogeneous environment. The observed coexistence of GASP mutants may result from the slow selection of GASP populations, or may indicate that different mutants can achieve close growth advantages by adopting different strategies. In this study, we aim to characterize survival and coexistence strategies of bacterial mutants in the long-term stationary phase with a simple model for bacterial population dynamics. In the model, for simplicity, we assume that one or two bacterial species (mutant strains) exist at the beginning of the incubation and ignore additional mutations during the incubation. In this way, we use the population dynamics of one or two strains to reflect characteristics of the long-term stationary phase. This is reasonable because the states that one GASP mutant dominates surviving cells and a younger GASP mutant gradually surrenders to, takes over, or coexists with an older dominating GASP mutant are representative in the long-term stationary phase.

The distribution of proteome among different physiological processes determines the bacterial exponential growth rate under various conditions [16–18]. Recent studies showed that proteome allocation also affects the competitive growth advantage when external resources are available [19], the death rate when external nutrients are depleted [20,21], and the growth-maintenance tradeoff from feast to famine [7]. The GASP mutants emerging in long-term stationary phase may also gain growth advantages by optimizing protein allocation. Here, we investigate how proteome allocation affects survival and coexistence strategies in the prolonged starvation.

The Gerland group discovered a constant death rate (exponential decay of cell viability) in carbon starvation, which they linked to the balance between nutrient demand by viable cells and nutrient supply by recycled dead cells [20]. They also found a correlation between cell growth rate and death rate (or maintenance rate) and proposed a mathematical model of proteome-based growth-death coupling to show the tradeoff between fast growth and long survival [7]. They emphasized the maintenance of viability rather than the regrowth of viable cells by consuming nutrients leaked from dead cells because no regrowth was detected in death phase cultures. However, the regrowth of viable cells by consuming recycling nutrients should be an important dynamic process in the long-term stationary phase. When a GASP mutant is emerged in the aged culture, the debris of dead cells will be the only nutrient source for the new GASP mutant growing and taking over the population. Macromolecules (e.g., proteins, DNA, lipids, and peptidoglycan) originated from dead cells can be degraded into small components for living cells to consume as nutrients [13,22–25]. Experiments show that some GASP mutants acquire growth competition fitness by improving the ability of using amino aids as sole carbon and energy sources [13,23]. DNA can also be used as the sole carbon and energy source for bacterial growth; some gene mutations make bacteria lose the ability to consume DNA and competitive growth advantage during prolonged stationary phase [24,25]. It suggests that the death of viable cells, the recycling of macromolecules from dead cells, and the regrowth of viable cells by consuming recycled nutrients should all be considered for characterizing population dynamics in the long-term stationary phase.

Takano *et al.* [6] constructed a kinetic model for describing the growth, death, and recycling of bacterial cells to account for the variation of surviving cell density during the 30-days cultivation. However, they assumed two complex functions to describe the dependence of growth and death rates on nutrient concentration and density of viable cells. Here we developed a simpler model to describe the growth, death, and recycling of the bacteria in long-term stationary phase by assuming constant death and recycling rates and a linear dependence of growth rate on nutrient concentration. With our model, we produced the population evolution of one or two species over time, which is consistent with representative experimental observations. Through analytical or numerical derivation, we obtained the extinction-survival-coexistence phase diagram of bacterial population in different cases (at steady state or in a limited detection time, with one or two species, sharing the same nutrient or using different nutrients). We also provided conditions of one species' survival and two species' coexistence in each case. The results show that our simple model is sufficient to characterize bacterial survival and coexistence strategies.

The bacteria can obtain fitness advantage by raising growth or recycling rate or reducing death rate. However, protein cost is required for all the processes of growth, maintenance, and recycling. Therefore the bacteria need to optimize the proteome allocation among these processes. Changes in growth rate or mortality under certain perturbations have been found to be associated with proteome redistribution [7,16–18,21]. As an extension, we linked growth, death, and recycling rates to proteomic fractions allocated to corresponding processes in the model for the long-term stationary phase. Through analytical or numerical derivation, we obtained effects of proteome allocation on the extinction-survival-coexistence phase diagram and the survival and coexistence conditions in different cases. The results suggest the tradeoff between processes of cell growth, maintenance-repair, and nutrient recycling which results from the limitation and optimization of protein allocation.

II. RESULTS

A. A growth-death-recycling kinetic model for one bacterial strain

In the long-term stationary phase of bacterial culture, the featured events include the death of viable cells, the recycling of dead cells into nutrient substrate and the growth (proliferation) of viable cells by consuming recycled nutrients [Fig. 1(a)]. To describe the long-term surviving kinetics of bacterial population simply, we make the following settings or assumptions. First, we partition bacterial culture into three coarse-grained parts: Viable cells, dead cells, and nutrients; viable cells can grow and proliferate by consuming recycled nutrients from dead cells; dead cells include cell debris that has not been broken into reusable nutrients; the initial

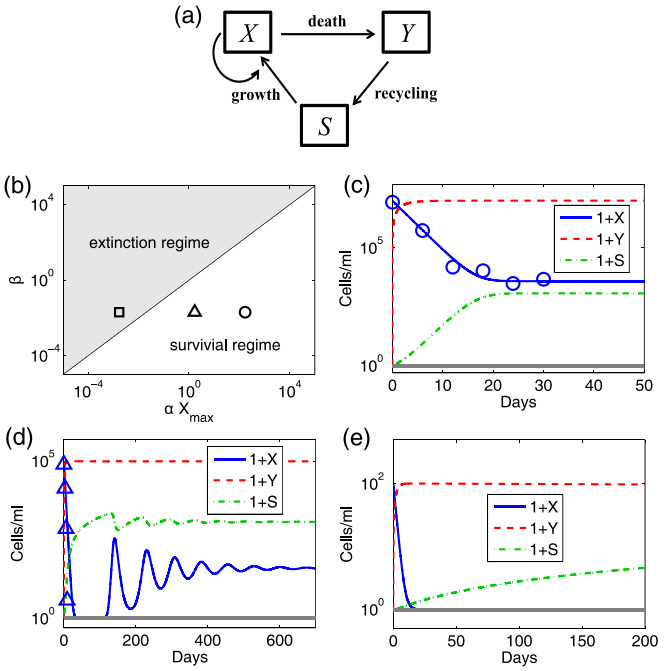

FIG. 1. The population dynamics of one bacterial strain shows the survival and extinction regimes at steady state, which can be determined by the ratio of β to $\alpha X_{\max}$. (a) Schematic illustration for the bacterial population dynamics: Viable cells (X) die into dead cells (Y) and grow by consuming nutrient substrate (S) recycled from dead cells (Y). (b) Phase diagram of bacterial survival density at steady state: When $\alpha X_{\max}/\beta > 1$, the bacteria survive; when $\alpha X_{\max}/\beta < 1$, the bacteria become extinct. The open circle, triangle, and square correspond to (c)–(e), respectively. [(c)–(e)] Three examples of the evolution of viable cells (X), dead cells (Y), nutrient substrate (S) with the time. The blue circles and triangles indicate the experimental viable cell densities from Takano *et al.* [6]. (c) and (d) show surviving population at steady state, while (e) shows the population becomes extinct before the steady state. At a steady state corresponding to (e), dead cells will be recycled into the nutrient completely, i.e., $Y = 0$ and $S = X_{\max}$. Parameters are listed in Appendix B.

culture includes only a fixed number of viable cells and the recycling of dead cells is the only source of nutrients; the recycled nutrients can be consumed for the growth (proliferation) or/and maintenance of viable cells [20]. Second, we ignore the mutation possibility, cell-to-cell variability, and complex composition of nutrients; the most limited nutrient is used to indicate all nutrients. Third, we assume that viable, dead, and reproduced cells have the same single-cell mass; nutrient substrate is in the unit of cells per volume.

When the culture includes only one bacterial strain, we use X to denote the density of viable cells, Y to denote the density of dead cells, and S to denote the concentration of nutrient substrate. Viable cells uptake the nutrient and grow with a rate $\mu S/(S + K_S)$. In the long-term stationary phase, only a small cell population are viable in the culture [1,8], which implies that the nutrient is limited to very low level, i.e., $S \ll K_S$. Thus $\mu S/(S + K_S) \approx \alpha S$, where $\alpha = \mu/K_S$. Living cells die with a rate β; dead cells are recycled into nutrients with a rate γ; recycled nutrients were consumed at a rate k_d that may depend on S to maintain one cell's energy dissipation [20]. Accordingly, the ODEs for describing changes in X, Y, and S with time are

$$\frac{dX}{dt} = \alpha SX - \beta X, \tag{1}$$

$$\frac{dY}{dt} = \beta X - \gamma Y, \tag{2}$$

$$\frac{dS}{dt} = \gamma Y - \alpha SX - k_d X. \tag{3}$$

The boundary conditions are $X, Y, S \geqslant 0$. If the growth term αSX is much smaller than other terms, and the total amount of dead cells and nutrients stay constant, i.e., $\frac{d(Y+S)}{dt} = 0$, we obtain $-\frac{1}{X}\frac{dX}{dt} \approx \beta \approx k_d$, which reflects the balance between nutrient demand for energy dissipation and nutrient supply from cell death. This situation is similar to the death phase scenario described by Schink *et al.* [20], in which no cell regrowth is detected and the death rate is determined based on the balance between maintenance cost and biomass recycling. However, regrowth (proliferation) by consuming recycled nutrients is a common feature of long-term starved bacteria (see Introduction), so we retain the growth term as well as the death and recycling terms in the model. If $k_d > 0$, the recyclable nutrients will be irreversibly consumed until the cell population becomes extinct (note that $\frac{d(X+Y+S)}{dt} = -k_d X$). If irreversible nutrient depletion is significant (k_d is large enough) during long-term starvation, the population will be reduced to a hard-to-detect level in a relatively short period of time, which conflicts with the long-term (e.g., >5 years' [1]) viability of the detected starving bacteria. Therefore k_d should be small enough during long-term starvation, which is consistent with experimental evidence that reduced maintenance rate leads to prolonged survival under carbon starvation [7]. In order to simplify the model and highlight the growth, death and recycling processes, we omit the slow and irreversible nutrient consumption for maintenance, i.e., let $k_d = 0$, in the following results (examples for effects of energy dissipation in the case of $k_d > 0$ on starving population dynamics is present in Appendix C). Thus Eqs. (1)–(3) satisfy the mass conversation [Fig. 1(a)], and we denote the total culture mass as $X_{\max}$.

For simplicity, we assume that α, β, and γ are constant. Thus the steady-state solution (X^*, Y^*, S^*) can be derived analytically. We analyzed the stability of each steady state by linearizing Eqs. (1)–(3) near the steady state point and deriving the characteristic root of the corresponding Jacobian matrix (Appendix A). When $\beta > \alpha X_{\max}$, there is only one steady state: $(0, 0, X_{\max})$, which is stable. This case corresponds to the extinction of the bacteria. When $\beta \leqslant \alpha X_{\max}$, there are two steady states: $(0, 0, X_{\max})$ (unstable) and $(\frac{\gamma}{\beta+\gamma}(X_{\max} - \frac{\beta}{\alpha}), \frac{\beta}{\beta+\gamma}(X_{\max} - \frac{\beta}{\alpha}), \frac{\beta}{\alpha})$ (stable). This case reflects the long-term survival of the bacteria. Figure 1(b) shows a survival-extinction phase diagram, where the diagonal $\beta = \alpha X_{\max}$ in the plot of β versus $\alpha X_{\max}$ separates survival and extinction regimes. The change in the growth rate constant α, total culture mass $X_{\max}$, or the death rate β shifts the bacterial population between the survival and extinction regimes [Figs. 1(b)–1(e)]. Simulations with different values of $X_{\max}$ show different evolutions of cell population and different final survival densities [Figs. 1(c)–1(e)], which basically

agrees with long-term cultivation experiments with different initial bacterial densities [6,26]. As shown in Figs. 1(c)–1(e), the fast (e.g., approximately exponential [20,26]) decay of viable cell density leads to the rapid accumulation of dead cells during early few days, while the slow recycling of dead cells causes the amount of recycled nutrient increases more slowly. When $X_{\max}$ is high, the nutrient can be recycled to an amount that meets the need of remaining viable cells in the population before it is extinct [e.g., Figs. 1(c) and 1(d)]; otherwise, the population becomes extinct before the nutrient is recycled enough [e.g., Fig. 1(e)]. Figures 1(c) and 1(d) present two survival instances with different population dynamics: The former exhibits monotonic changes, whereas the latter exhibits fluctuating changes. They are similar to the overdamping and underdamping phenomena in electrical circuits. Because of the limitation on the measurement time and precision, the seeming 'extinction' state in the experiment may correspond to a steady state in the survival regime rather than in the extinction regime [Fig. 1(d)]. Figure 1(e) presents a theoretical extinction example. Note that dead cells shown in Fig. 1(e) are still being recycled into nutrients after 200 days, although there are no viable cells, which reflects the slowness of the recycling process.

B. Incorporation of proteome allocation into the growth-death-recycling kinetic model for one bacterial strain

The limitation of bacterial cell resources leads to the tradeoff between the resources allocated to various cellular processes. Scott *et al.* systematically investigated the trade-offs between metabolic and translation processes under nutrient and translation limitations and proposed a simple mathematic model to describe proteome reallocation between these processes [16]. To study the effect of stress on protein maturation, we previously extended their model to include two extra processes, protein maturation and degradation, thus dividing the proteome into more sectors [18]. Here, we consider the allocation of protein resources among cell growth (including uptake, metabolic, and translational processes), maintenance (including death factors' resistance and repair processes), and recycling of death cells (including various degradation processes). Analogous to the idea of previous models [16,18], we divide the proteome into three classes: P_1 (for growth), P_2 (for maintenance), and P_3 (for recycling) and use ϕ_1, ϕ_2, and ϕ_3 to denote the corresponding proteomic fractions. Note that this proteome partitioning is highly coarse-grained. The biological consideration of partitioning is that one gene can be classified into one sector according to its main function and change modes under particular stresses [16–18].

Transporters, metabolic enzymes, and ribosomes are limited for cellular growth, so the growth rate constant can be expressed as a linear function of ϕ_1 [16–18], i.e.,

$$\alpha = a(\phi_1 - \phi_{1,0}), \tag{4}$$

where the new growth rate constant a is independent of proteomic allocation fractions and $\phi_{1,0}$ denotes the inactive or inefficient part of ϕ_1. $\phi_{1,0}$ includes the proteome fraction for inactive ribosomes and the proteome cost due to the lack of tRNA required for saturated translation speed [27,28]. $\phi_{1,0}$ may depend on growth rate as well as the proteome fraction for inactive ribosomes [28]. We tested the linear dependence of $\phi_{1,0}$ on growth rate, which results in the α-ϕ_1 relationship in a form similar to Eq. (4) with constant $\phi_{1,0}$ (see Appendix E). Therefore we assume that $\phi_{1,0}$ is a constant independent of growth rate.

P_2-class proteins maintain the normal physiological state of cells to reduce the death rate. They include molecular chaperons, repair enzymes, and other proteins that contribute to the maturation, stability, and integrity of biological macromolecules. In cells, the synthesis of those macromolecules should be much more laborious than the production of P_2-class proteins. Economically, cells will tend to minimize the abnormal maturation, instability, and incompleteness of laboriously produced macromolecules by preparing enough P_2-class proteins. The Michaelis-Menten equation is widely used to represent the kinetics of enzymatic reactions, and the action of an inhibitor can be represented by $K/(K + I)$, where I is the inhibitor concentration and K is the Michaelis constant. Thus we consider that β is a Michaelis-Menten function of ϕ_2, i.e.,

$$\beta = b\frac{K_m}{K_m + \phi_2}, \tag{5}$$

where the death rate constant b and Michaelis constant K_m do not depend on proteomic allocation fractions. Equation (5) quantitatively describes the inhibitory effect of P_2-class proteins on the death rate at high yet subsaturation levels. It is similar to the formula for the relationship between aberrant protein maturation flux and proteomic fraction for chaperons, which has been used to explain the growth rate independence of chaperon proteomic fraction ($\sim$0.05) from mass spectrometry [18].

P_3-class proteins required for the recycling of dead cells include degradation enzymes for proteins, RNA, DNA, lipids, and other biological macromolecules. Just as metabolic enzymes are limited to external nutrients [16–18], these degradation enzymes should also be limited to the recyclable macromolecules. Otherwise, the building blocks of the macromolecules will accumulate to wasteful levels, unable to offset the cost of producing these degrading enzymes. Thus the recycling rate γ can be represented as a linear function of ϕ_3, that is,

$$\gamma = c\phi_3. \tag{6}$$

The recycling rate constant c does not depend on proteomic allocation fractions. This is similar to that the aberrant proteins' degradation flux linearly depends on the proteomic fraction for proteases, which has been used to account for the growth rate independence of protease proteomic fraction ($\sim$0.02) from mass spectrometry [18]. The normalization condition for ϕ_1, ϕ_2, and ϕ_3 is $\phi_1 + \phi_2 + \phi_3 = 1$.

The bacteria suffering from long-term starvation have the opportunity to regain exogenous nutrients. In order to increase the probability of survival under the starvation or other common stresses, the bacterial population should tend to maximize the number of viable cells. Here, we assume that bacteria achieve this object by optimizing protein allocation among P_1, P_2, and P_3. When $\beta \geqslant \alpha X_{\max}$, the bacterial population will be always extinct. When $\beta < \alpha X_{\max}$, the optimization object is to maximize the function $X^*(\phi_1, \phi_2) =$

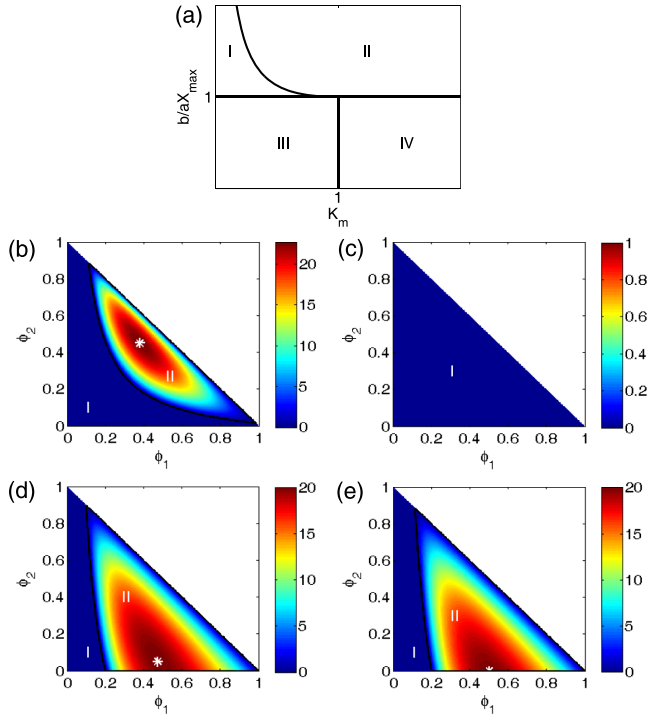

FIG. 2. The effect of protein allocation on the population survival of one bacterial strain. (a) Four distinct regimes exists for the survival space and the optimal survival point. Regime I represents that the survival space satisfies $\phi_{1,2,3} > 0$ and the optimal survival point satisfies $\phi^{\rm opt}_{1,2,3} > 0$. Regime II represents a zero survival space. Regime III represents that $\phi_{1,3} > 0, \phi_2 \geqslant 0, \phi^{\rm opt}_{1,2,3} > 0$. Regime IV represents that $\phi_{1,3} > 0, \phi_2 \geqslant 0, \phi^{\rm opt}_{1,3} > 0$, and $\phi^{\rm opt}_2 = 0$. [(b)–(e)] The examples of regimes I–IV shown in (a), respectively. The colorbar shows the steady-state survival density. The black line represents the border between the survival regime (white II) and the extinction regime (white I). The white star indicates the optimal survival point. Parameters: $a = 0.009$ [(b) and (c)] or 0.05 ml/(cell h) [(d) and (e)]; $b = 1\ {\rm h}^{-1}$; $c = 1\ {\rm h}^{-1}$; $K_m = 0.1$ (b), 0.9 [(c) and (d)], or 1.2 (e).

$\frac{c(1-\phi_1-\phi_2)}{bK_m/(K_m+\phi_2)+c(1-\phi_1-\phi_2)}(X_{\rm max} - \frac{bK_m}{a\phi_1(K_m+\phi_2)})$, where $\phi_1, \phi_2 \geqslant 0$ and $\phi_1 + \phi_2 \leqslant 1$ (notice that $\phi_1 + \phi_2 + \phi_3 = 1$ has been used).

Each set of proteomic allocation fractions (ϕ_1, ϕ_2, ϕ_3) must satisfies $\phi_{1,2,3} \geqslant 0$ and $\phi_1 + \phi_2 + \phi_3 = 1$, which defines a feasible space. With each set of proteomic allocation fractions, we can analytically derive the corresponding steady state. We define a survival space in which the density of viable cells is nonzero at steady state, and the optimal survival point $(\phi^{\rm opt}_1, \phi^{\rm opt}_2, \phi^{\rm opt}_3)$, which gives the maximal steady-state density of living cells. Considering the difference in survival space or optimal survival point, we obtained four distinct regimes (see Fig. 2): (I) when $1 < \frac{b}{aX_{\rm max}} \leqslant \frac{(1+K_m)^2}{4K_m}$ and $K_m < 1$, $\phi_{1,2,3}$ and $\phi^{\rm opt}_{1,2,3}$ are nonzero in the survival space [e.g., Fig. 2(b)]; (II) when $K_m < 1$ and $\frac{b}{aX_{\rm max}} > \frac{(1+K_m)^2}{4K_m}$, or when $K_m \geqslant 1$ and $\frac{b}{aX_{\rm max}} > 1$, the survival space does not exist [e.g., Fig. 2(c)]; (III) when $b \leqslant aX_{\rm max}$ and $K_m < 1$, $\phi_{1,3}$ and $\phi^{\rm opt}_{1,2,3}$ are nonzero in the survival space [e.g., Fig. 2(d)]; and (IV) when $b \leqslant aX_{\rm max}$ and $K_m \geqslant 1$, $\phi_{1,3}$ and $\phi^{\rm opt}_{1,3}$ are nonzero, and $\phi^{\rm opt}_2 = 0$ in the survival space [e.g., Fig. 2(e)]. The factors causing cell death may increase the death rate constant b or Michaelis constant K_m. According to above results, bacteria have different strategies of proteomic allocation in response to different effects of death factors on b and K_m. If the death rate constant is larger than growth rate constant times the total culture mass (i.e., $b > aX_{\rm max}$), the bacteria will tend to allocate a nonzero proteomic fraction to maintenance processes for reducing the death rate [Fig. 2(b)]. However, if death rate constant is large enough to satisfy $\frac{b}{aX_{\rm max}} > \frac{(1+K_m)^2}{4K_m}$, or the Michaelis constant is not smaller than 1 (i.e. $K_m \geqslant 1$) in addition to $b > aX_{\rm max}$, the death factor is hard to alleviate and the bacteria will become extinct no matter how they allocate the proteome [Fig. 2(c)]. If the death rate constant is not larger than growth rate constant times the total culture mass (i.e., $b \leqslant aX_{\rm max}$), bacteria will have a wider proteomic allocation space to survive, and even they can leave the death to happen by minimizing protein cost for maintenance to zero [Fig. 2(d)]. If, in addition, the Michaelis constant is not smaller than 1 (i.e., $K_m \geqslant 1$), the zero maintenance cost will be the optimal choice [Fig. 2(e)]. In conclusion, above results indicate that protein reallocation is one effective mechanism for bacteria to survive in long-term starvation.

C. A growth-death-recycling model for two bacterial strains sharing recycling nutrients

To study the long-term coexistence strategies of different bacterial strains, we consider that two bacterial strains (Nos. 1 and 2) are mixed and incubated in the same container for a long time. We develop a growth-death-recycling model to describe population dynamics for two species sharing recycling nutrients as below. Use X_1 and X_2 to denote densities of corresponding viable cells, Y_1 and Y_2 to denote densities of dead cells, and S to denote the concentration of recycled nutrient substrate (in the unit of cells per volume) from the dead debris of the two strains. A schematic diagram is shown by Fig. 3(a). The ODEs for population dynamics of the two strains are

$$\frac{dX_1}{dt} = \alpha_1 S X_1 - \beta_1 X_1, \tag{7}$$

$$\frac{dY_1}{dt} = \beta_1 X_1 - \gamma_1 Y_1, \tag{8}$$

$$\frac{dX_2}{dt} = \alpha_2 S X_2 - \beta_2 X_2, \tag{9}$$

$$\frac{dY_2}{dt} = \beta_2 X_2 - \gamma_2 Y_2, \tag{10}$$

$$\frac{dS}{dt} = \gamma_1 Y_1 - \alpha_1 S X_1 + \gamma_2 Y_2 - \alpha_2 S X_2. \tag{11}$$

where $X_1, Y_1, X_2, Y_2, S \geqslant 0$ and $X_1 + Y_1 + X_2 + Y_2 + S = X_{\rm max}$.

The steady-state solution $(X_1^*, Y_1^*, X_2^*, Y_2^*, S^*)$ can be derived analytically. We analyzed the stability of each steady state by linearizing Eqs. (7)–(11) near the fixed points and deriving the characteristic root of the corresponding Jacobian matrix (Appendix A). When $X_{\rm max} \leqslant \min(\beta_1/\alpha_1, \beta_2/\alpha_2)$, there is only one steady state $(0, 0, 0, 0, X_{\rm max})$, which is stable. It corresponds to the case in which both strains are extinct [e.g., Fig. 3(c)]. When $\beta_1/\alpha_1 < \min(X_{\rm max}, \beta_2/\alpha_2)$, the

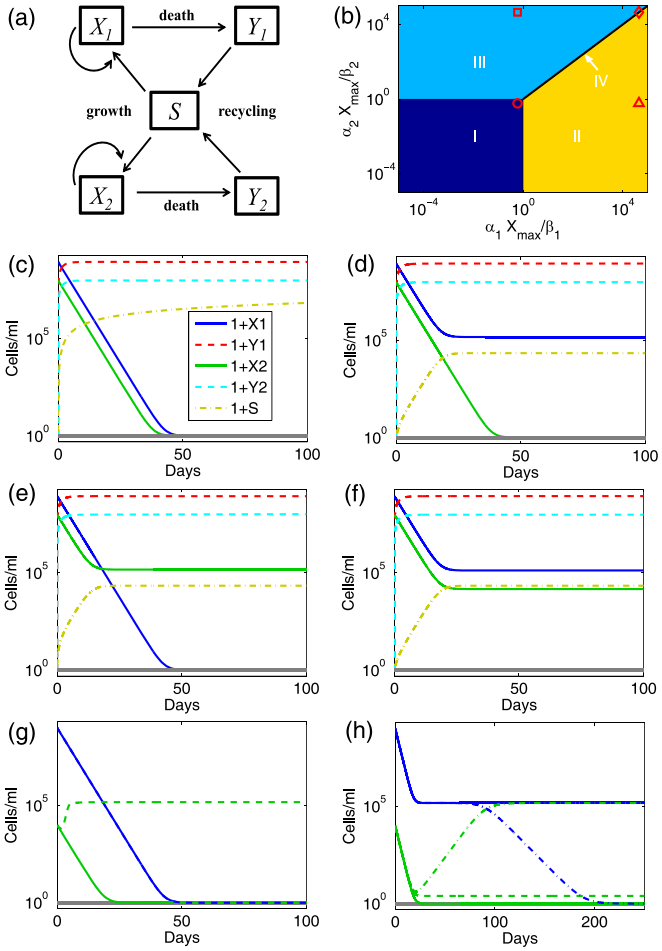

FIG. 3. Population dynamics of two strains sharing the recycling nutrient. (a) Schematic illustration for the population dynamics of two bacterial strains sharing the nutrient substrates. Viable cells of strains 1 and 2 (X_1 and X_2) grow by consuming the same nutrient substrate (S), which is recycled from dead cells of strains 1 and 2 (Y_1 and Y_2). (b) Phase diagram of four regimes for the survival strain number. Regimes I-IV represent the cases of the coextinction of both strains, only strain 1 surviving, only strain 2 surviving, and co-survival of both strains. [(c)–(f)] The evolution of viable cells (X_1 and X_2), dead cells (Y_1 and Y_2), nutrient substrate (S) with the time, corresponding to red circle, triangle, square, and diamond in regimes I–IV shown in (B). (g) If the survivability of strain 1 which occupies the majority of the population satisfies the extinct condition i.e., $SF_1 = \alpha_1 X_{\max}/\beta_1 < 1$, strain 2 as the minority affects little the survival density of strain 1 (e.g., overlapping solid blue and dashed blue lines), no matter the survivability of strain 2 satisfies $SF_2 = \alpha_2 X_{\max}/\beta_2 > 1$ (e.g., green dashed line) or <1 (e.g., green solid line). (h) If strain 1 satisfies $SF_1 > 1$, strain 2 overwhelms strain 1 when $SF_2 > SF_1$ (e.g., dash-dotted blue and dash-dotted green lines), surrenders to strain 1 when $SF_2 < SF_1$ (e.g., solid blue and solid green lines), and coexists with strain 1 when $SF_2 = SF_1$ [e.g., dashed blue (overlapping solid blue line) and dashed green lines].

stable steady state is $(\frac{\gamma_1(X_{\max}-\beta_1/\alpha_1)}{\beta_1+\gamma_1}, \frac{\beta_1(X_{\max}-\beta_1/\alpha_1)}{\beta_1+\gamma_1}, 0, 0, \beta_1/\alpha_1)$, which means that strain 2 all die, while strain 1 finally survives [e.g., Fig. 3(d)]. When $\beta_2/\alpha_2 < \min(X_{\max}, \beta_1/\alpha_1)$, the stable steady state is $(0, 0, \frac{\gamma_2(X_{\max}-\beta_2/\alpha_2)}{\beta_2+\gamma_2}, \frac{\beta_2(X_{\max}-\beta_2/\alpha_2)}{\beta_2+\gamma_2}, \beta_2/\alpha_2)$, which indicates that strain 1 is extinct, while strain 2 survives [e.g., Fig. 3(e)]. When $\beta_1/\alpha_1 = \beta_2/\alpha_2 < X_{\max}$, the stable steady state is $(X_1^*, \frac{\beta_1}{\gamma_1}X_1^*, C_0 X_1^{*\frac{\alpha_1}{\alpha_2}}, C_0\frac{\beta_2}{\gamma_2}X_1^{*\frac{\alpha_1}{\alpha_2}}, \frac{\beta_1}{\alpha_1})$, where $C_0 = X_2(0)/X_1^{\frac{\alpha_1}{\alpha_2}}(0)$ and X_1^* can be determined by solving the equation $X_1^* + C_0 X_1^{*\frac{\alpha_1}{\alpha_2}} = \frac{X_{\max}-\beta_1/\alpha_1}{1+\beta_1/\gamma_1}$. In this case, two strains coexist at steady state and their densities at steady state are dependent on initial densities [e.g., Fig. 3(f)]. Thus steady states of population dynamics of strains 1 and 2 define four distinct regimes based on ratios $\alpha_1 X_{\max}/\beta_1$ and $\alpha_2 X_{\max}/\beta_2$ [Fig. 3(b)]: (I) both strains become extinct, (II) only strain 1 survives, (III) only strain 2 survives, and (IV) both strains survive. As shown by Fig. 3(b), the coexistence of strains 1 and 2 occurs only on the line $\alpha_1 X_{\max}/\beta_1 = \alpha_2 X_{\max}/\beta_2 > 1$, i.e., $\alpha_1/\beta_1 = \alpha_2/\beta_2 > 1/X_{\max}$. These competition modes of two strains are similar to those observed in competition experiments of mixing "aged" and "young" cultures [11,12]. Note that initial conditions do not affect the phase diagram [Fig. 3(b)], which is determined by the total density ($X_{\max}$), growth rate constants (α_1 and α_2), and death rate constants (β_1 and β_2). However, initial densities of viable cells [$X_1(0)$ and $X_2(0)$] may affect steady-state densities. When one bacterial strain shares the same nutrients with another, a higher initial viable cell density can lead to a higher steady-state viable cell density [Fig. 3(f)]. This reflects the continuity of competitive advantage.

According to the above results, the factor $\alpha_i X_{\max}/\beta_i$ reflects the survivability of strain i. If the survivability factor (abbreviated to SF) of one strain is higher than 1, the population only containing this strain will survive; otherwise, the population will die out. Above results and Fig. 3(b) have shown specific conditions under which strain 2 surrenders to, coexists with, or replaces strain 1. To better reflect the emergence of GASP mutant in the long-term starvation, we simulated the population dynamics by fixing SF of strain 1 (SF_1), which initially occupies the majority of the population, and varying SF of strain 2 (SF_2), which is the minority at the beginning [Figs. 3(g) and 3(h)]. When strain 1 satisfies $SF_1 < 1$, strain 1 will die out independent of the survivability of strain 2, and strain 2 will take over the population if $SF_2 \geqslant 1$ [Fig. 3(g)]. When $SF_1 \geqslant 1$, the survivability's diversity of the emergent strain 2 leads to that strain 2 surrenders to (if $SF_2 < SF_1$, i.e., $\alpha_2/\beta_2 < \alpha_1/\beta_1$), coexists with (if $SF_2 = SF_1$, i.e., $\alpha_2/\beta_2 = \alpha_1/\beta_1$), or overwhelms strain 1 (if $SF_2 > SF_1$, i.e., $\alpha_2/\beta_2 > \alpha_1/\beta_1$) [Fig. 3(h)]. This roughly repeats different competition modes of "young" and "aged" cultures [11,12] and more clearly points to the condition of the emergence of GASP mutant.

Next, we consider the effect of protein allocation on the survival and coexistence strategies to show the tradeoff between cellular growth, maintenance, and recycling. For the sake of convenience, we assume that the two strains only differ in proteomic fractions. Use $\phi_i (i \in 1, 2, 3)$ and $\psi_i (i \in 1, 2, 3)$ to denote proteomic fractions allocated to growth, maintenance, or recycling for strains 1 and 2, respectively. As similarly done for the case of one strain, we formulate the growth, maintenance, and recycling rates as: $\alpha_1 = a\phi_1$, $\beta_1 = b\frac{K_m}{K_m+\phi_2}$, $\gamma_1 = c\phi_3$, $\alpha_2 = a\psi_1$, $\beta_2 = b\frac{K_m}{K_m+\psi_2}$, $\gamma_2 = c\psi_3$, where a, b, and c are rate constants and K_m is Michaelis

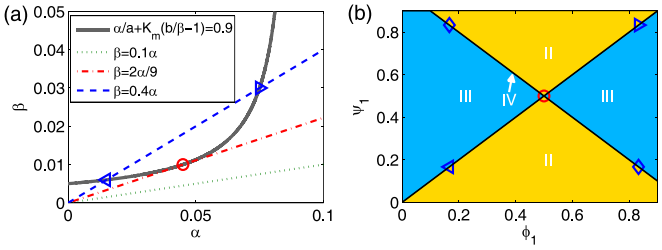

FIG. 4. Tradeoff between cell growth and maintenance and coexistence of two strains sharing the recycling nutrient at steady state under the constraint $\gamma_1 = \gamma_2 = \text{const}$ (i.e., $\phi_3 = \psi_3 = \text{const}$). (a) The coexistence conditions of two strains show that the coexisting strains can have different compromised growth and death rates (i.e. different values of α and β). $\gamma = 0.1c$. (b) The ϕ_1-ψ_1 phase diagram of two strains' survival and coexistence. II–IV denote the regimes in which only strain 1 survives, only strain 2 survives, and two strains co-survive, respectively. The red circle corresponds to that both strains choose the α-β values at the red circle shown in (a). The left (right)-pointed triangle corresponds to that both strains choose the α-β values at the left (right)-pointed triangle shown in (a). The diamonds correspond to that the two strains choose the α-β values at the left and right-pointed triangles shown in (a), respectively. Parameters: $\phi_3 = \psi_3 = 0.1$, $a = 0.09$ ml/(cell h), $b = 0.05\ \text{h}^{-1}$, and $K_m = 0.1$.

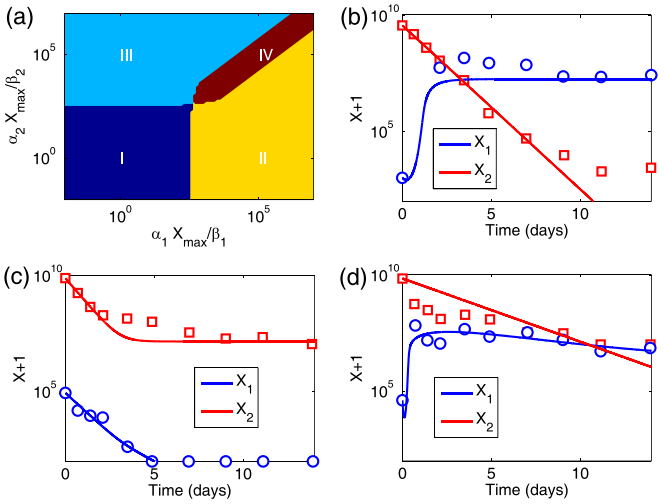

FIG. 5. Phase diagram and some examples of population dynamics for two strains sharing the recycling nutrient under a limited time. (a) Phase diagram of the co-growth of two strains (1 and 2). Four regimes are formed: (I) both strains are extinct; (II) strain 1 survives, whereas strain 2 is extinct; (III) strain 2 survives, whereas strain 1 is extinct; and (IV) both strains survive. α is the adjustable parameter. [(b)–(d)] Examples for regimes II-IV. Blue circles and red squares denote experimental data from [29]. Parameters are present in Appendix B.

constant. Under the constraints of normalization conditions $\phi_1 + \phi_2 + \phi_3 = 1$ and $\psi_1 + \psi_2 + \psi_3 = 1$, the degree of freedom of the system is 4. To provide an example to show the dependence of two strains' coexistence on allocation fractions, we consider additional constraints: $\phi_3 = \psi_3 = 0.1$, which means that the two strains have the same proteomic fraction for the recycling. Accordingly, $\gamma_1 = \gamma_2 = 0.1c$ and $\phi_1 + \phi_2 = \psi_1 + \psi_2 = 0.9$. The degree of freedom is reduced to 2. We consider ϕ_1 and ψ_1 as the two free parameters. According to the above results, the coexistence of the two strains requires $\alpha_1/\beta_1 = \alpha_2/\beta_2 > 1/X_{\text{max}}$. Thus the specific coexistence condition here is that $(\alpha_1,\ \beta_1)$ and $(\alpha_2,\ \beta_2)$ should be located at the intersection between the straight line $\beta = k\alpha$ $(k < X_{\text{max}})$ and the curve $\alpha/a + K_m(b/\beta - 1) = 0.9$ [Fig. 4(a)]. The curve reflects the tradeoff between growth and maintenance, while the two intersections [see triangles in Fig. 4(a)] show the possibility of the coexistence of two strains differing in the compromised growth and death rates. Corresponding to the two intersections, there are four solutions of $(\phi_1,\ \psi_1)$ [see triangles and diamonds in Fig. 4(b)]. Here we consider X_{max} large enough so that $1/X_{\text{max}} \approx 0$. Finally, the coexistence points constitute two diagonal lines: $\psi_1 = \phi_1$ and $\psi_1 + \phi_1 = 0.9 + K_m$ [see phase diagram in Fig. 4(b)]. The coexistence points on the line $\psi_1 + \phi_1 = 0.9 + K_m$ suggest that the coexisting strains can have different proteomic allocation fractions. The case in which only strain 1 survives requires that $\alpha_1/\beta_1 > \alpha_2/\beta_2$, i.e., $(\phi_1 - \psi_1)(\phi_1 + \psi_1 - 0.9 - K_m) < 0$, corresponding to the top and bottom regions separated by coexistence lines in Fig. 4(b). The case in which only strain 2 survives requires that $\alpha_2/\beta_2 > \alpha_1/\beta_1$, i.e., $(\phi_1 - \psi_1)(\phi_1 + \psi_1 - 0.9 - K_m) > 0$, corresponding to the left and right regions separated by coexistence lines in Fig. 4(b).

In above results, the survival of bacterial population is determined under steady state. However, two limitations exist in detecting bacterial survival in the experiment. One is the limitation of the measurement time, that is, the measurement time may be not enough to reach the steady state (see above). Actually, a too long measurement will get into a state in which the mutation frequently occur. However, our model cannot describe the population dynamics with frequent mutations. The other is the limitation of the detection precision, namely, there is a nonzero minimal survival density that can be detected. In the wet-lab, therefore, the survival of bacteria is usually determined by observing whether the survival density is detectable at the final detection time. The effect of the limited detection time depends on initial values and the measurement duration. If we use small enough death rates (e.g., $\beta_1 = \beta_2 = 0.001\ \text{h}^{-1}$) while changing the growth rates, and let $\gamma_1 = \gamma_2 = 3 \times 10^{-6}\ \text{h}^{-1}$, $X_1(0) = X_2(0) = X_{\text{max}}/2 = 0.5 \times 10^9$ cells/ml, $Y_1(0) = Y_2(0) = S(0) = 0$, the limited detection time is 14 days and the minimal detectable survival density is 100, both strains will survive in the entire ranges of $\alpha_1 X_{\text{max}}/\beta_1$ and $\alpha_2 X_{\text{max}}/\beta_2$ shown in Fig. 3(b). This is understandable because the duration before the population becomes extinct (the density is lower than the minimal detectable) (extinction time) is much longer than the total detection time. The extinction time can be reduced by increasing the minimal detectable survival density or the death rate. With higher death rates (e.g., $\beta_1 = \beta_2 = 0.05\ \text{h}^{-1}$) (other parameters have the same values as above), four regimes emerge and the coexistence regime is pencil-shaped [Fig. 5(a)] rather than a line [Fig. 3(b)]. Moreover, the results for different initial densities of viable and dead cells (Appendix D and Fig. 10) indicate that initial conditions can affect the phase diagram as well as final densities. However, if the initial conditions are not extremely abnormal (such as no viable cells of strain 1 or 2),

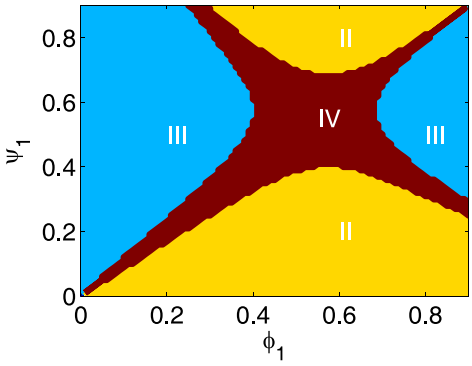

FIG. 6. The ϕ_1-ψ_1 phase diagram of the survival and coexistence of two strains sharing the recycling nutrient under a limited time and a constraint $\gamma_1 = \gamma_2 = \text{const}$ (i.e., $\phi_3 = \psi_3 = \text{const}$). II–IV denote the regimes in which only strain 1 survives, only strain 2 survives, and two strains cosurvive, respectively. See related parameters in Appendix B.

the four regimes remain and the coexistence regime is still pen shaped (Fig. 10). Finally, we can adjust the parameters to compare theoretical results to three experimental data sets of cell viability as a function of the time [29], which correspond to three different regimes: (1) strain 1 survives, whereas strain 2 is extinct [Fig. 5(b)], (2) strain 1 is extinct, whereas strain 2 survives [Fig. 5(c)], and (3) both strains survive [Fig. 5(d)]. One complex case is also observed in the experiment [29], in which one strain conquers another strain in the early stage, but the advantage of the first strain is surpassed by the second strain in the late stage. This case implies that a genetic change leading to a larger growth advantage occurs in the second strain. Our model does not involve the mutation, so it cannot explain this complex case directly.

With the above-used limited detection time (14 days) and the minimal detectable survival density (100), we reproduced the survival-extinction phase diagram of the two strains based on the proteomic allocation (i.e., ϕ_1 and ψ_1). The results show that the coexistence regime becomes an irregular star shape (Fig. 6) instead of a cross [Fig. 4(b)]. Above results indicate that bacterial survival and coexistence spaces observed in actual experimental conditions may be different from that obtained at the steady state.

D. The growth-death-recycling model for two bacterial strains using different recycling nutrients

Evidence shows that bacteria strains especially GASP mutants can use amino acids or DNA as the sole carbon and energy source [13,23–25]. In addition, different GASP mutants may prefer different categories of amino acids [13,23]. The *sgaA* GASP mutation can lead to a loss of consuming oligopeptides but an increase in utilizing amino acids monomers [30]. These results suggest that different bacterial strains may uptake and metabolize different recycling nutrients in prolonged starvation. To study this case, we construct a model with two bacterial strains consuming two different types of recycling nutrients. Use S_1 and S_2 to denote concentrations of limiting nutrients (in the unit of cells per volume), X_1 and X_2 to denote densities of viable cells, and Y_1 and Y_2 to denote densities of dead cells for strains 1 and 2, respectively.

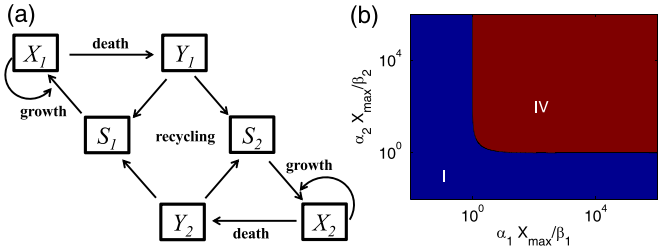

FIG. 7. Schematic diagram and phase diagram for two strains using different recycling nutrients. (a) Schematic diagram. X_i, Y_i, and S_i are the density of viable cells, density of dead cells, and concentration of nutrient source of strain i ($i \in \{1, 2\}$), respectively. (b) The $\alpha_1 X_{\max}/\beta_1$-$\alpha_2 X_{\max}/\beta_2$ phase diagram of the survival and coexistence of the two strains, independent of specific values of the parameters. "I" and "IV" indicate coextinction and coexistence regimes, respectively.

A relevant schematic diagram is shown by Fig. 7(a). The corresponding ODEs are

$$\frac{dX_1}{dt} = \alpha_1 S_1 X_1 - \beta_1 X_1, \tag{12}$$

$$\frac{dY_1}{dt} = \beta_1 X_1 - \gamma_1 Y_1, \tag{13}$$

$$\frac{dX_2}{dt} = \alpha_2 S_2 X_2 - \beta_2 X_2, \tag{14}$$

$$\frac{dY_2}{dt} = \beta_2 X_2 - \gamma_2 Y_2, \tag{15}$$

$$\frac{dS_1}{dt} = -\alpha_1 S_1 X_1 + \rho_1 \gamma_1 Y_1 + (1-\rho_2)\gamma_2 Y_2, \tag{16}$$

$$\frac{dS_2}{dt} = -\alpha_2 S_2 X_2 + \rho_2 \gamma_2 Y_2 + (1-\rho_1)\gamma_1 Y_1, \tag{17}$$

where $X_i, Y_i, S_i \geqslant 0$ ($i \in \{1, 2\}$), $0 \leqslant \rho_i \leqslant 1$ ($i \in \{1, 2\}$), and $\sum_{i=1}^{2}(X_i + Y_i + S_i) = X_{\max}$. ρ_i represents the mass fraction of dead cells recycled to the nutrient S_i, while $1 - \rho_i$ represents the remaining fraction recycled to the other nutrient. When $\rho_1 = \rho_2 = 0$, all resources circulate between strains 1 and 2. When $\rho_1 = \rho_2 = 1$, no resources flow between the two strains, equivalent to two isolated single strain systems. Below we only consider $\rho_1, \rho_2 \neq 1$. When $0 < \rho_1, \rho_2 < 1$, a portion of resources circulate between the two strains. The circulation of resources between the two strains implies strong cooperation between them, as opposed to competition for resources while consuming the same nutrient. The steady-state solution $(X_1^*, Y_1^*, X_2^*, Y_2^*, S_1^*, S_2^*)$ of Eqs. (12)–(17) can be derived analytically. There are two possible steady-state solutions: $SS_1 = (0, 0, 0, 0, S_1^*, X_{\max} - S_1^*)$ and $SS_2 = (\frac{X_C}{\beta_1 \xi}, \frac{X_C}{\gamma_1 \xi}, \frac{\eta X_C}{\beta_2 \xi}, \frac{\eta X_C}{\gamma_2 \xi}, \frac{\beta_1}{\alpha_1}, \frac{\beta_2}{\alpha_2})$, where $X_C = X_{\max} - \frac{\beta_1}{\alpha_1} - \frac{\beta_2}{\alpha_2}$, $\xi = 1/\beta_1 + \eta/\beta_2 + 1/\gamma_1 + \eta/\gamma_2$, and $\eta = (1-\rho_1)/(1-\rho_2)$. If $X_{\max} - \beta_2/\alpha_2 \leqslant S_1^* \leqslant \beta_1/\alpha_1$, SS_1 is stable; otherwise, the solution is unstable. If $\alpha_1 > \beta_1$, $\alpha_2 > \beta_2$, and $X_{\max} > \beta_1/\alpha_1 + \beta_2/\alpha_2$, SS_2 exists, and it is stable at least when γ_1, γ_2, A, and B is close to zero. We use H to denote the Harmonic mean of $\alpha_1 X_{\max}/\beta_1$ and $\alpha_2 X_{\max}/\beta_2$. When $H \leqslant 2$, both strains are extinct, whereas when $H > 2$, both strains survive. This forms an coextinction-coexistence phase diagram of two strains using different nutrients as shown by Fig. 7(b). In the phase

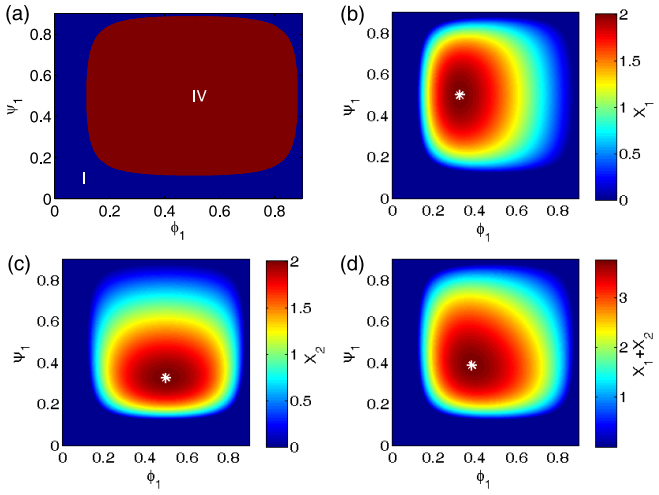

FIG. 8. Tradeoff between cell growth and maintenance in the coexistence of two strains using different recycling nutrients under the constraint $\gamma_1 = \gamma_2 = \text{const}$ (i.e., $\phi_3 = \psi_3 = \text{const}$). (a) The ϕ_1-ψ_1 phase diagram of the survival and coexistence of two strains. "I" and "IV" indicate co-extinction and coexistence regimes, respectively. [(b)–(d)] The survival density of strain 1 (X_1), strain 2 (X_2), or their sum ($X_1 + X_2$) as a function of ϕ_1 and ψ_1. White stars indicate corresponding maximum points. Parameters: $X_{\max} = 10^7$cells/ml, $\phi_3 = \psi_3 = 0.1$, $K_m = 0.1$, $a = 8 \times 10^{-7}$ ml/(cell h), $b = 6\,\text{h}^{-1}$, and $c = 10^{-5}\,\text{h}^{-1}$.

diagram, there are only two regimes: (I) both strains are extinct and (IV) both strains survive. To gain the coexistence, unlike in the case of two strains consuming the same nutrient, two strains consuming different nutrients are not required to have the same growth rate/death rate ratio. It indicates a higher coexistence freedom when different bacteria strains consume different nutrients. Note that, as in the case of sharing the same nutrient, the phase diagram is determined by the total density and growth rate and death rate constants, independent of initial conditions. The steady state is affected by rate constants (α_i, β_i, and γ_i), total mass $X_{\max}$, and mass fractions, but not by specific initial values. This reflects the robustness of this system, compared with the system of two strains sharing the nutrient that may depend on initial conditions (see above).

When two strains use different nutrients, the ϕ_1-ψ_1 phase diagram also consists of two regimes (I) both strains are extinct; and (IV) both strains survive. The regime (IV) has a square shape with arc edges [Fig. 8(a)]. This also indicates a higher coexistence freedom when the strains consume different nutrients, compared with the case of the strains consuming the same nutrient. The maxima of the density of strain 1, the density of strain 2 and their sum are not at the same (ϕ_1, ψ_1) point. If both strains tend to optimize their own density, neither of them can reach the maximum of the density, and their densities' sum cannot reach the maximum, either. If the two strains cooperate with each other, they can achieve the maximal sum of their densities. This is similar to the prisoner's dilemma. It suggests that the cooperation between different GASP mutants may be an effective strategy to increase the survival probability of the entire population in the long-term stationary phase culture.

III. DISCUSSION

In this study, we modelled the growth-death-recycling dynamics of one or two strains and found the survival condition of one strain and cosurvival condition of two strains. We also, for the first time, characterize effects of proteome allocation on the survival and coexistence strategies. The results suggest the tradeoff between growth, maintenance, and recycling. Our model could be extended to describe the population dynamics and coexistence of more than two microbial species under the long-term starvation or other stresses. The related results could be checked by well-designed experiments. When revising this manuscript, we found that the model of Takano *et al.* [6] had been simplified by Shoemaker *et al.* [31] into a form similar to our single strain model. But neither their model nor the one of Takano *et al.* has been used to study the co-survival of multiple strains and the influence of proteome allocation.

Many regulatory mechanisms underlie the tradeoff of growth-maintenance-recycling processes [1,13]. One well-known candidate is the regulation of the level of alternative sigma factor σ^S, which can modulate the tradeoff by changing the allocation of proteome between different processes [18,32]. The emergence of GASP mutations in *rpoS* [1,13] points to a tradeoff adjustment in adaptation to the state variation of bacterial populations and nutrients. In the early stage (e.g., early stationary phase and death phase), bacteria tend to cease growth and maintain a long survival, whereas, in the late stage (e.g., prolonged stationary phase), bacteria tend to increase proteomic fractions for the recycling of dead cells and the regrowth of viable cells. The shift from persistence and resistance of nongrowth cells to scavenging recycling nutrients and resuming growth is analogous to the change from cooperation to defection in the prisoner's dilemma [33].

This study highlights the tradeoff underlying the prolonged starvation. Tradeoff between growth, maintenance, and recycling may exist when bacteria suffer other long-term stresses. For example, a linear correlation between bacterial growth rate and lysis rate mediated by β-lactam has been observed under various additional stresses modulating cell growth [34], suggesting a universal tradeoff between growth and maintenance.

In the model, two underlying assumptions are the spatially uniform and constant environmental conditions (no external nutrient supply and no change in temperature). It has been found that the space-segregation [15] or seasonal environment [14] can also facilitate the coexistence of different bacterial strains. The model could be advanced to quantify effects of the heterogeneity of nutrient or other signaling factors in space or time on bacterial survival and coexistence.

Our work points to a bacterial evolution strategy in the long-term shortage of nutrients, i.e., the GASP mutant can acquire growth advantage by optimizing proteomic fractions for growth, maintenance, and recycling. The successive emergence of GASP mutants in long-term starvation cultivation is a good target for studying the evolution of microbial communities [12,13]. It might be possible to involve mutations in our model or other similar models.

Nongrowth cells need to consume nutrients (or energy) to maintain their viability, which has been described by some theoretical models [20,35–37]. Schink *et al.* [20] proposed

that during the death phase, nutrients provided by the lysis of dead cells are in balance with nutrients (free energy) needed to maintain the viability of nongrowth cells. Based on this assumption, they explained the exponential decay of population viability in death phase and the increase in death rate with the overexpression of a wasteful protein [20]. The quantification of microbiological maintenance is still in debate [36,37]. The proposition of Schink *et al.* [20] on the nutrient supply-demand balance needs further detailed testing. As mentioned above, our model for one strain [Eqs. (1)–(3)] decays to the scenario described by Schink *et al.* [20] when $\alpha SX \approx 0$ and $\frac{d(Y+S)}{dt} = 0$. However, when we do not consider energy dissipation [i.e., $k_d = 0$ in Eq. (3)], the results of our model can also reflect the exponential decay during the death phase. In the framework of our model without energy dissipation, if the rate of recycling dead cells to nutrients that are usable for viable cells is very slow and the initial nutrient concentration is close to zero, the concentration of recycled nutrients in the dead phase will be very low [e.g., the case before 15 days shown in Fig. 1(c)]. Thus the growth term αSX in Eq. (1) can be ignored, in agreement with experimental evidence that no growing cells were observed in the death phase [20]. Finally, according to Eq. (1), the density of viable cells will decrease with the time exponentially [e.g., the case before 15 days shown in Fig. 1(c)]. With our model involving proteome allocation, the decrease in death rate with the overexpression of a wasteful protein can be easily explained by the decrease in the proteomic fraction allocated to maintaining cell viability.

Some phenomena, such as viable but nonculturable (VBNC) state or stationary phase contact-dependent inhibition (SCDI) [2,38], that have been observed in experiments reflect special survival strategies in response to the prolonged starvation. The VBNC cells stay dormant in most cases, and recover from the dormancy only under special conditions [2]. At the VBNC or dormant state, the strain has a nearly zero growth rate but a very long survival, corresponding to the case of $\phi_1 = \phi_3 \approx 0$, $\phi_2 \approx 1$, and $K_m \sim 0$ in our model [see Eqs. (4)–(6)]. This reflects an extreme tradeoff between growth, maintenance and recycling. In the SCDI phenomenon, emerging strains kill the parent strain or inhibit the growth of the parent strain [38]. The inhibitory relationship between two strains can be added in our model, in which case the extinction-survival phase diagram should vary with the inhibitory strength.

IV. CONCLUSION

Here, we developed a kinetic model to describe the survival, death, and recycling of bacterial strains. With the model, we studied the population dynamics of one bacterial strain or two bacterial strains sharing the same nutrients or using different nutrients, produced the survival-extinction-coexistence phase diagram at the steady state or in the limited measurement time, and determined the conditions of one strain's survival and two strains' coexistence. We also showed effects of constraints and optimization of proteome allocation between processes for cell growth, death, and recycling nutrients on the phase diagrams, which reflect the tradeoff between theses processes. Our results quantitatively characterize bacterial survival and coexistence strategies during the prolonged starvation. Especially, our results suggest that bacteria could achieve growth advantages by regulating tradeoff between cell growth, death and recycling processes via protein reallocation.

ACKNOWLEDGMENTS

This work was supported by the Strategic Priority Program of Chinese Academy of Sciences (No. XDA17010504), the National Natural Science Foundation of China (Grants No. 12274426 and No. 12047503).

APPENDIX A: THE STABILITY ANALYSIS OF EACH SYSTEM

The stability of the system at each steady state can be obtained by deriving the sign of the characteristic roots (the real part, if the root is a complex number).

1. The system with one strain

For the system described by Eqs. (1)–(3), the Jacobian matrix at the steady state (X^*, Y^*, S^*) is

$$J = \begin{bmatrix} \alpha S^* - \beta & 0 & \alpha X^* \\ \beta & -\gamma & 0 \\ -\alpha S^* & \gamma & -\alpha X^* \end{bmatrix}. \tag{A1}$$

The characteristic equation $J - \lambda E = 0$ has three roots: $\lambda_{1,2,3} = \alpha S^* - \beta$, $-\gamma$, and $-\alpha X^*$. Equations (1)–(3) have two possible steady-state solutions: $SS_1 = (0, 0, X_{\max})$ and $SS_2 = (\frac{\beta(X_{\max} - \beta/\alpha)}{\gamma+\beta}, \frac{\gamma(X_{\max} - \beta/\alpha)}{\gamma+\beta}, \beta/\alpha)$. (1) The steady state SS_1 always exists. When $\alpha X_{\max} \leqslant \beta$, $\lambda_{1,2,3} \leqslant 0$, so SS_1 is stable; when $\alpha X_{\max} > \beta$, $\lambda_1 > 0$, so SS_1 is unstable. (2) The steady state SS_2 exists only when $\alpha X_{\max} > \beta$; when $\alpha X_{\max} > \beta$, $\lambda_{1,2,3} \leqslant 0$, so SS_2 is stable.

2. The system with two strains sharing the same nutrient

For the system described by Eqs. (7)–(11), the Jacobian matrix at the steady state $(X_1^*, Y_1^*, X_2^*, Y_2^*, S^*)$ is

$$J = \begin{bmatrix} \alpha_1 S^* - \beta_1 & 0 & 0 & 0 & \alpha_1 X_1^* \\ \beta_1 & -\gamma_1 & 0 & 0 & 0 \\ 0 & 0 & \alpha_2 S^* - \beta_2 & 0 & \alpha_2 X_2^* \\ 0 & 0 & \beta_2 & -\gamma_2 & 0 \\ -\alpha_1 S^* & \gamma_1 & -\alpha_2 S^* & \gamma_2 & -\alpha_1 X_1^* - \alpha_2 X_2^* \end{bmatrix}. \tag{A2}$$

The characteristic equation $J-\lambda E=0$ has five roots. Equations (7)–(11) have four possible steady-state solutions:

$$SS_1=(0,0,0,0,X_{\max}),$$

$$SS_2=\left(0,0,\frac{\gamma_2\left(X_{\max}-\frac{\beta_2}{\alpha_2}\right)}{\beta_2+\gamma_2},\frac{\beta_2\left(X_{\max}-\frac{\beta_2}{\alpha_2}\right)}{\beta_2+\gamma_2},\frac{\beta_2}{\alpha_2}\right),$$

$$SS_3=\left(\frac{\gamma_1\left(X_{\max}-\frac{\beta_1}{\alpha_1}\right)}{\beta_1+\gamma_1},\frac{\beta_1\left(X_{\max}-\frac{\beta_1}{\alpha_1}\right)}{\beta_1+\gamma_1},0,0,\frac{\beta_1}{\alpha_1}\right),$$

$$SS_4=\left(X_1^*,\frac{\beta_1}{\gamma_1}X_1^*,C_0X_1^{*\frac{\alpha_1}{\alpha_2}},C_0\frac{\beta_2}{\gamma_2}X_1^{*\frac{\alpha_1}{\alpha_2}},\frac{\beta_1}{\alpha_1}\right),$$

where $C_0=X_2(0)/X_1^{\frac{\alpha_1}{\alpha_2}}(0)$ and X_1^* can be determined by solving the equation $X_1^*+C_0X_1^{*\frac{\alpha_1}{\alpha_2}}=\frac{X_{\max}-\beta_1/\alpha_1}{1+\beta_1/\gamma_1}$.

Next, we give the existence and stability of these four steady-state solutions. (1) The steady state SS_1 always exists. At the steady state SS_1, the characteristic roots $\lambda_{1,2,3,4,5}=0,-\gamma_1,-\gamma_2,\alpha_1X_{\max}-\beta_1,\alpha_2X_{\max}-\beta_2$. When $X_{\max}\leqslant\min(\beta_1/\alpha_1,\beta_2/\alpha_2)$, $Rel(\lambda_{2,3,4,5})<0$, SS_1 is stable; otherwise, SS_1 is unstable. (2) The steady state SS_2 exists when $\beta_2/\alpha_2<X_{\max}$. At the steady state SS_2, the characteristic roots $\lambda_{1,2,3,4,5}=0,-\gamma_1,\frac{\alpha_1}{\alpha_2}\beta_2-\beta_1,\frac{-(B+\gamma_2)-\sqrt{\Delta}}{2},\frac{-(B+\gamma_2)+\sqrt{\Delta}}{2}$, where $\Delta=(B-\gamma_2)^2-4B\beta_2$ and $B=\frac{\gamma_2(\alpha_2X_{\max}-\beta_2)}{\gamma_2+\beta_2}$. When $\frac{\beta_2}{\alpha_2}<\frac{\beta_1}{\alpha_1}$, $Rel(\lambda_{2,3,4,5})<0$, SS_2 is stable; otherwise, SS_2 is unstable. (3) The steady state SS_3 exists when $\beta_1/\alpha_1<X_{\max}$. At the steady state SS_3, the characteristic roots $\lambda_{1,2,3,4,5}=0,-\gamma_2,\frac{\alpha_2}{\alpha_1}\beta_1-\beta_2,\frac{-(A+\gamma_1)-\sqrt{\Delta}}{2},\frac{-(A+\gamma_1)+\sqrt{\Delta}}{2}$, where $\Delta=(A-\gamma_1)^2-4A\beta_1$ and $A=\frac{\gamma_1(\alpha_1X_{\max}-\beta_1)}{\gamma_1+\beta_1}$. When $\frac{\beta_1}{\alpha_1}<\frac{\beta_2}{\alpha_2}$, $Rel(\lambda_{2,3,4,5})<0$, SS_3 is stable; otherwise, SS_3 is unstable. (4) SS_4 exists when $\beta_1/\alpha_1=\beta_2/\alpha_2<X_{\max}$. The characteristic equation is $\lambda^2f_3(\lambda)=0$, where $f_3(\lambda)=(\lambda+\gamma_1)(\lambda+\gamma_2)(\lambda+A+B)+B\beta_2(\lambda+\gamma_1)+A\beta_1(\lambda+\gamma_2)$ (A and B are defined as above). So $\lambda_{1,2}=0$ and $\lambda_{3,4,5}$ are given by the cubic equation $f_3(\lambda)=0$. It can be demonstrated that $\mathrm{Rel}(\lambda_{3,4,5})<0$ (see below), so SS_4 is always stable.

The equation $f_3(\lambda)=0$ can be transformed to $\lambda^3+b\lambda^2+c\lambda+d=0$, where $b=\gamma_1+\gamma_2+A+B>0$, $c=\gamma_1\gamma_2+(A+B)(\gamma_1+\gamma_2)+A\beta_1+B\beta_2>0$, and $d=\gamma_1\gamma_2(A+B)+B\beta_2\gamma_1+A\beta_1\gamma_2>0$. It has $bc-d>0$. A cubic equation with one variable has at least one real root. We assume that $f_3(\lambda)=0$ has a real root λ_1, then it can be factorized into $(\lambda-\lambda_1)(\lambda+e\lambda+f)=0$, where e and f are real numbers. So $b=e-\lambda_1$, $c=f-e\lambda_1$, and $d=-f\lambda_1$. Combining the above inequality formulas, we have $\lambda_1<0$, $e<0$, and $f<0$, and then $\mathrm{Rel}(\lambda_{1,2,3})<0$. Therefore SS_4 is stable.

3. The system with two strains using different nutrients

For the system described by Eqs. (12)–(17), the Jacobian matrix at the steady state $(X_1^*,Y_1^*,X_2^*,Y_2^*,S_1^*,S_2^*)$ is

$$J=\begin{bmatrix}\alpha_1S_1^*-\beta_1 & 0 & 0 & 0 & \alpha_1X_1^* & 0\\ \beta_1 & -\gamma_1 & 0 & 0 & 0 & 0\\ 0 & 0 & \alpha_2S_2^*-\beta_2 & 0 & 0 & \alpha_2X_2^*\\ 0 & 0 & \beta_2 & -\gamma_2 & 0 & 0\\ -\alpha_1S_1^* & \rho_1\gamma_1 & 0 & (1-\rho_2)\gamma_2 & -\alpha_1X_1^* & 0\\ 0 & (1-\rho_1)\gamma_1 & -\alpha_2S_2^* & \rho_2\gamma_2 & 0 & -\alpha_2X_2^*\end{bmatrix}. \tag{A3}$$

The characteristic equation $J-\lambda E=0$ has six roots. Equations (12)–(17) have two possible steady-state solutions: $SS_1=(0,0,0,0,S_1^*,X_{\max}-S_1^*)$ and $SS_2=(\frac{X_C}{\beta_1\xi},\frac{X_C}{\gamma_1\xi},\frac{\eta X_C}{\beta_2\xi},\frac{\eta X_C}{\gamma_2\xi},\frac{\beta_1}{\alpha_1},\frac{\beta_2}{\alpha_2})$, where $X_C=X_{\max}-\frac{\beta_1}{\alpha_1}-\frac{\beta_2}{\alpha_2}$, $\xi=1/\beta_1+\eta/\beta_2+1/\gamma_1+\eta/\gamma_2$, and $\eta=\frac{1-\rho_1}{1-\rho_2}$. Next, we give the existence and stability of these two steady-state solutions. (1) The steady-state SS_1 always exists. At SS_1, the characteristic roots are $\lambda_{1,2,3,4,5,6}=0,0,-\gamma_1,-\gamma_2,\alpha_1S_1^*-\beta_1,\alpha_2(X_{\max}-S_1^*)-\beta_2$. when $X_{\max}-\beta_2/\alpha_2\leqslant S_1^*\leqslant\beta_1/\alpha_1$, $\lambda_{1,2,3,4,5,6}\leqslant0$, SS_1 is stable; otherwise, it is unstable. (2) The steady-state SS_2 exists when $X_{\max}>\beta_1/\alpha_1+\beta_2/\alpha_2$. The characteristic equation is $g_3(\lambda)h_3(\lambda)-AB\beta_1\beta_2(1-\rho_1)(1-\rho_2)\gamma_1\gamma_2=0$, where $g_3(\lambda)=\lambda(\lambda+\gamma_1)(\lambda+A)+A\beta_1\lambda+A\beta_1\gamma_1(1-\rho_1)$ and $h_3(\lambda)=\lambda(\lambda+\gamma_2)(\lambda+B)+B\beta_2\lambda+B\beta_2\gamma_2(1-\rho_2)$ and $A=\alpha_1X_1^*$ and $B=\alpha_2X_2^*$. If $A,B,\gamma_1,\gamma_2\approx0$, then $g_3(\lambda)\approx0$ and $h_3(\lambda)\approx0$. Equation $g_3(\lambda)=0$ can be transformed to $\lambda^3+b\lambda^2+c\lambda+d=0$, where $b=\gamma_1+A>0$, $c=A(\beta_1+\gamma_1)>0$, and $d=A\beta_1\gamma_1(1-\rho_1)>0$. It has $bc-d>0$. So $Rel(\lambda)<0$, i.e. $g_3(\lambda)=0$ has three roots with negative real part. In the same way, $h_3(\lambda)=0$ also has three roots with negative real part. The characteristic roots all have negative real part. So SS_2 is stable.

APPENDIX B: SOME PARAMETERS USED FOR FIGURES

Parameters for Figs. 1(c)–1(e): $X(0)=X_{\max}=10^7$ cells/ml (c), 10^5 cells/ml (d), or 10^2 cells/ml (e); $Y(0)=S(0)=0$; $\alpha=1.7\times10^{-5}$ ml/(cell h); $\beta=0.02\ \mathrm{h}^{-1}$; and $\gamma=7.74\times10^{-6}\ \mathrm{h}^{-1}$. In particular, the parameters for Figs. 1(c) and 1(d) were determined based on experimental data of Takano *et al.* [6]. $X_{\max}$ was set to the initial experimental cell density. At the early stage, the death dominates the population dynamics, so β was determined from the first two experimental data points (t_1,X_1) and (t_2,X_2) by the formula $-\ln(X_2/X_1)/(t_2-t_1)$; the β values obtained from experimental data for Figs. 1(c) and 1(d) were averaged. The steady-state viable cell density for Fig. 1(c) was estimated to be the average of the last two experimental densities, which gives a quantitative relationship between α and γ,

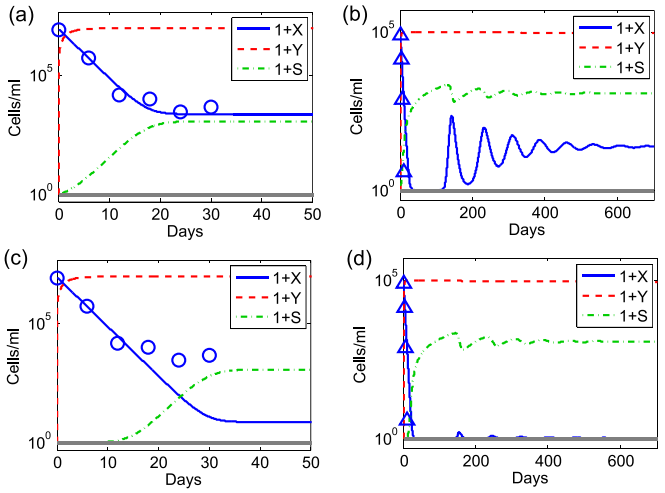

FIG. 9. Dependence of starving population dynamics on the rate at which a cell consumes nutrients due to energy dissipation (k_d^*). Parameters except k_d^* are the same to those for Figs. 1(c) and 1(d), respectively. [(a) and (b)] A small k_d^* value ($k_d^* = 1 \times 10^{-5}$ h^{-1}) affects population dynamics little, compared with the case of $k_d^* = 0$. [(c) and (d)] A large k_d^* value ($k_d^* = 0.01$ h^{-1}) leads to a bigger decrease in the density of living cells, compared with the case of $k_d^* = 0$.

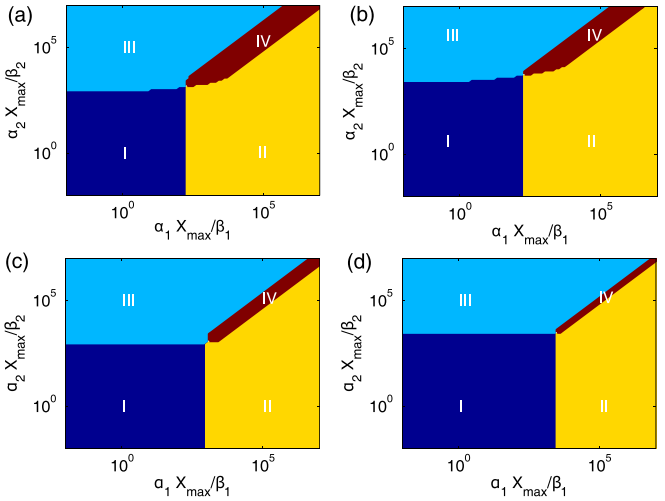

FIG. 10. Effects of initial densities on the phase diagram of two strains (1 and 2) sharing the recycling nutrient in a limited time. Four regimes are formed with different initial densities: (I) both strains are extinct; (II) strain 1 survives, whereas strain 2 is extinct; (III) strain 2 survives, whereas strain 1 is extinct; and (IV) both strains survive. Parameters are the same as those used for Fig. 5(a), except the initial densities for viable and dead cells: $X_1(0) = 0.99X_{\max}$, $X_2(0) = 0.01X_{\max}$, $Y_1(0) = Y_2(0) = 0$ (a); $X_1(0) = (1 - 10^{-9})X_{\max}$, $X_2(0) = 10^{-9}X_{\max}$, $Y_1(0) = Y_2(0) = 0$ (b); $X_1(0) = X_2(0) = 0.01X_{\max}$, $Y_1(0) = Y_2(0) = 0.49X_{\max}$ (c); $X_1(0) = X_2(0) = 10^{-9}X_{\max}$, and $Y_1(0) = Y_2(0) = (0.5 - 10^{-9})X_{\max}$ (d).

i.e., $\frac{\gamma}{\beta+\gamma}(X_{\max} - \beta/\alpha) \approx \frac{X_5+X_6}{2}$. Then γ can be expressed as a function of α, i.e., $\gamma = A\beta/(1-A)$, where $A = \frac{X_5+X_6}{2(X_{\max}-\beta/\alpha)}$. Thus we determined the unique free parameter α by fitting experimental cell densities as a function of time using the least square method. Finally, we fixed γ according to the above function.

Parameters for Figs. 3(c)–3(h): $X_{\max} = 10^9$ cells/ml; $Y_1(0) = Y_2(0) = S(0) = 0$; $\beta_1 = \beta_2 = 0.02$ h^{-1}; $\gamma_1 = \gamma_2 = 3 \times 10^{-6}$ h^{-1}; $X_1(0) = 0.9X_{\max}$ [(c)–(f)] or $(1 - 10^{-5})X_{\max}$ [(g) and (h)]; $X_2(0) = 0.1X_{\max}$ [(c)–(f)] or $10^{-5}X_{\max}$ [(g) and (h)]; $\alpha_1 = 1.2 \times 10^{-11}$ [(c), (e), and (g)] or 9×10^{-7} ml/(cell·h) [(d), (f), and (h)]; $\alpha_2 = 1.2 \times 10^{-11}$ [(c), (d), solid blue and solid green lines in (g) and (h)], 9×10^{-7} [(e), (f), dashed blue and dashed green lines in (g) and (h)], or 1.2×10^{-6} ml/(cell h) [dash-dotted blue and dash-dotted green lines in (h)].

Parameters for Fig. 5(a): $X_{\max} = 10^9$ cells/ml; α_1 and α_2 are variables; $\beta_1 = \beta_2 = 0.05$ h^{-1}; $\gamma_1 = \gamma_2 = 3 \times 10^{-6}$ h^{-1}; $X_1(0) = X_2(0) = X_{\max}/2$; $Y_1(0) = Y_2(0) = S(0) = 0$; the limited detection time is 14 days; the minimal detectable survival density is 100.

Parameters for Figs. 5(b)–5(d): $X_1(0) = 1.04 \times 10^3$ (b), 9.12×10^4 (c), or 4.15×10^4 cells/ml (d); $X_2(0) = 3.85 \times 10^9$ (b), 8.06×10^9 (c), or 7.36×10^9 cells/ml (d); $Y_1(0) = Y_2(0) = S(0) = 0$; $\alpha_1 = 4 \times 10^{-4}$ (b), 4.84×10^{-6} (c), or 0.021 ml/(cell h) (d); $\alpha_2 = 2.2 \times 10^{-6}$ (b), 1.5×10^{-5} (c), or 1.5×10^{-5} ml/(cell h) (d); β_1=0.068 (b), 0.067 (c), or 1.2 h^{-1} (d); $\beta_2 = 0.068$ (b), 0.085 (c), or 0.027 h^{-1} (d); $\gamma_1 = 4.5 \times 10^{-4}$ (b), 1.58×10^{-4} (c), or 4.5×10^{-4} h^{-1} (d); $\gamma_2 = 4.5 \times 10^{-4}$ (b), 1.58×10^{-4} (c), or 0.011 h^{-1} (d). Initial values were determined based on the experimental data at the first time point. We fixed the other parameters by adding extra constraints (according to characteristics of experimental data or arbitrarily) and fitting the experimental data (least-square method was used). For panel (b), we considered additional constraints $\beta_1 = \beta_2$ and $\gamma_1 = \gamma_2$ (arbitrarily); β_2 (and then β_1) was determined by fitting experimental X_2 values (red squares) at the first three time points; the average of X_1 values at the last two time points were assigned to $\frac{\gamma_1}{\beta_1+\gamma_1}(X_2(0) - \frac{\beta_1}{\alpha_1})$, with which, α_1 and α_2 (and then γ_1 and γ_2) were fixed by fitting all related experimental data. For panel (c), β_1 and β_2 were determined by fitting experimental X_1 and X_2 values at the first three time points; the average of X_2 values at the last two time points were assigned to $\frac{\gamma_2}{\beta_2+\gamma_2}(X_2(0) - \frac{\beta_2}{\alpha_2})$, with which, α_2 (and then γ_2) were fixed by fitting experimental data for strain 2 (red squares); the additional constraint $\gamma_1 = \gamma_2$ was also used (arbitrarily); finally, α_1 was fixed by fitting all related experimental data. For panel (d), β_2 was determined by fitting the experimental data for strain 2 at the first six time points (red squares); α_2 (γ_1) was assigned the same value as for panel (b)[(a)] (arbitrarily); finally, α_1, β_1, and γ_2 were determined by fitting all related experimental data.

Parameters for Fig. 6: $X_{\max} = 10^7$ cells/ml, $X_1(0) = X_2(0) = X_{\max}/2$; $Y_1(0) = Y_2(0) = S(0) = 0$; $\phi_3 = \psi_3 = 0.1$, $a = 0.27$ ml/(cell h), $b = 0.15$ h^{-1}, $c = 3 \times 10^{-5}$ h^{-1}, $K_m = 0.5$; the limited detection time is 14 days; the minimal detectable survival density is 100 cells/ml.

APPENDIX C: THE EFFECT OF ENERGY DISSIPATION

The rate at which a cell consumes nutrients due to energy dissipation is expressed by k_d in Eq. (3). Here we consider $k_d(> 0)$ as a function of the nutrient concentration S: $k_d(S) =$

$k'_d \frac{S}{S+K_d}$. At high nutrient deficiencies, $S \ll K_d$ and $k_d(S) \approx k^*_d S$, where $k^*_d = k'_d/K_d$. Our results show that the effect of energy dissipation on population dynamics depends on the size of k^*_d: When k^*_d is small, the dynamics changes little compared with the case without energy dissipation (i.e., $k^*_d = 0$); when k^*_d is large, the dynamic changes are significant and the living cells are reduced to a lower level compared with the case of $k^*_d = 0$ (Fig. 9).

APPENDIX D: THE DEPENDENCE OF PHASE DIAGRAM OF TWO STRAINS SHARING THE RECYCLING NUTRIENT IN A LIMITED TIME ON THEIR INITIAL DENSITIES

In order to test the influence of initial densities on the phase diagram of two strains competing for growth over a limited period of time, we used different values of $X_1(0)$, $X_2(0)$, $Y_1(0)$, and $Y_2(0)$, to regenerate the phase diagram, in comparison with the case of $X_1(0) = X_2(0) = 0.5X_{\max}$ and $Y_1(0) = Y_2(0) = 0$ shown in Fig. 5(a). The results show that the phase diagram, especially the coexistence region, changes more or less with the change of initial conditions (Fig. 10). However, the dependence of the phase diagram on initial conditions does not change our main conclusion: Four distinct regimes can be formed, and the coexistence regime is still a pen-shaped area [except under extremely abnormal initial conditions, such as $X_1(0)$ or $X_2(0) = 0$].

APPENDIX E: THE EFFECT OF THE GROWTH RATE DEPENDENCE OF $\phi_{1,0}$

As a source of $\phi_{1,0}$, inactive ribosomes were found to decrease with increasing growth rate during slow growth [28]. Therefore $\phi_{1,0}$ may also vary with growth rate. Here we consider the linear growth rate dependence of $\phi_{1,0}$, as Dai *et al.* did for the proteome fraction devoted to inactive ribosomes [28], i.e., $\phi_{1,0} = \phi_{1,0^*} - b\alpha$. Substituting this relationship into Eq. (4), we obtain $\alpha = \frac{a}{1-ab}(\phi_1 - \phi_{1,0^*})$, which has the same form as Eq. (4).

[1] S. E. Finkel, Long-term survival during stationary phase: Evolution and the gasp phenotype., Nat. Rev. Microbiol. **4**, 113 (2006).

[2] J. M. Navarro Llorens, A. Tormo, and E. Martínez-García, Stationary phase in gram-negative bacteria, FEMS Microbiol. Rev. **34**, 476 (2010).

[3] V. Bačun-Družina, A. Butorac, J. Mrvčić, T. L. Dragičević, and V. Stehlik-Tomas, Bacterial stationary-phase evolution, Food Technol. Biotechnol. **49**, 13 (2011).

[4] H. Bremer and P. P. Dennis, Modulation of chemical composition and other parameters of the cell by growth rate, in *Escherichia coli and Salmonella: Cellular and Molecular Biology*, Vol. 2, edited by F. C. Neidhardt, R. Curtiss III, J. L. Ingraham, E. C. C. LIN, K. B. Low, B. Magasanik, W. S. Reznikoff, M. Riley, M. Schaechter, and H. E. Umbarger, 2nd ed. (American Society for Microbiology, Washington, DC, USA, 1996), pp. 1553–1569.

[5] S. Klumpp, Z. Zhang, and T. Hwa, Growth rate-dependent global effects on gene expression in bacteria, Cell **139**, 1366 (2009).

[6] S. Takano, B. J. Pawlowska, I. Gudelj, T. Yomo, and S. Tsuru, Density-dependent recycling promotes the long-term survival of bacterial populations during periods of starvation, mBio **8**, e02336-16 (2017).

[7] E. Biselli, S. J. Schink, and U. Gerland, Slower growth of escherichia coli leads to longer survival in carbon starvation due to a decrease in the maintenance rate, Mol. Syst. Biol. **16**, e9478 (2020).

[8] E. A. Steinhaus and J. M. Birkeland, Studies on the life and death of bacteria. i. the senescent phase in aging cultures and the probable mechanisms involved, J. Bacteriol. **38**, 249 (1939).

[9] K. E. Kram, A. L. Henderson, and S. E. Finkel, Escherichia coli has a unique transcriptional program in long-term stationary phase allowing identification of genes important for survival, mSystems **5**, e00364-20 (2020).

[10] N. R. Ratib, F. Seidl, I. M. Ehrenreich, and S. E. Finkel, Evolution in long-term stationary-phase batch culture: Emergence of divergent escherichia coli lineages over 1,200 days, mBio **12**, e03337-20 (2021).

[11] M. Zambrano, D. Siegele, M. Almiron, A. Tormo, and R. Kolter, Microbial competition: Escherichia coli mutants that take over stationary phase cultures, Science **259**, 1757 (1993).

[12] S. E. Finkel and R. Kolter, Evolution of microbial diversity during prolonged starvation, Proc. Natl. Acad. Sci. USA **96**, 4023 (1999).

[13] E. R. Zinser and R. Kolter, Escherichia coli evolution during stationary phase, Res. Microbiol. **155**, 328 (2004).

[14] D. E. Rozen, N. Philippe, J. Arjan de Visser, R. E. Lenski, and D. Schneider, Death and cannibalism in a seasonal environment facilitate bacterial coexistence, Ecol. Lett. **12**, 34 (2009).

[15] J. E. Keymer, P. Galajda, G. Lambert, D. Liao, and R. H. Austin, Computation of mutual fitness by competing bacteria, Proc. Natl. Acad. Sci. USA **105**, 20269 (2008).

[16] M. Scott, C. W. Gunderson, E. M. Mateescu, Z. Zhang, and T. Hwa, Interdependence of cell growth and gene expression: Origins and consequences., Science **330**, 1099 (2010).

[17] S. Hui, J. M. Silverman, S. S. Chen, D. W. Erickson, M. Basan, J. Wang, T. Hwa, and J. R. Williamson, Quantitative proteomic analysis reveals a simple strategy of global resource allocation in bacteria, Mol. Syst. Biol. **11**, 784 (2015).

[18] Q. Zhang, R. Li, J. Li, and H. Shi, Optimal allocation of bacterial protein resources under nonlethal protein maturation stress, Biophys. J. **115**, 896 (2018).

[19] L. Pacciani-Mori, S. Suweis, A. Maritan, and A. Giometto, Constrained proteome allocation affects coexistence in models of competitive microbial communities, ISME J. **15**, 1458 (2021).

[20] S. J. Schink, E. Biselli, C. Ammar, and U. Gerland, Death rate of e. coli during starvation is set by maintenance cost and biomass recycling, Cell Syst. **9**, 64 (2019).

[21] S. Schink, C. Ammar, Y.-F. Chang, R. Zimmer, and M. Basan, Analysis of proteome adaptation reveals a key role of the bacterial envelope in starvation survival, Mol. Syst. Biol. **18**, e11160 (2022).

[22] C. Mason, J. Bryers, and G. Hamer, Activity, death and lysis during microbial growth in a chemostat, Chem. Eng. Commun. **45**, 163 (1986).

[23] E. R. Zinser and R. Kolter, Mutations enhancing amino acid catabolism confer a growth advantage in stationary phase, J. Bacteriol. **181**, 5800 (1999).

[24] S. E. Finkel and R. Kolter, Dna as a nutrient: Novel role for bacterial competence gene homologs, J. Bacteriol. **183**, 6288 (2001).

[25] V. Palchevskiy and S. E. Finkel, Escherichia coli competence gene homologs are essential for competitive fitness and the use of DNA as a nutrient, J. Bacteriol. **188**, 3902 (2006).

[26] A. Phaiboun, Y. Zhang, B. Park, and M. Kim, Survival kinetics of starving bacteria is biphasic and density-dependent, PLoS Comput. Biol. **11**, e1004198 (2015).

[27] S. Klumpp, M. Scott, S. Pedersen, and T. Hwa, Molecular crowding limits translation and cell growth, Proc. Natl. Acad. Sci. USA **110**, 16754 (2013).

[28] X. Dai, M. Zhu, M. Warren, R. Balakrishnan, V. Patsalo, H. Okano, J. R. Williamson, K. Fredrick, Y.-P. Wang, and T. Hwa, Reduction of translating ribosomes enables escherichia coli to maintain elongation rates during slow growth, Nat. Microbiol. **2**, 16231 (2016).

[29] B. Yeiser, E. D. Pepper, M. F. Goodman, and S. E. Finkel, Sos-induced DNA polymerases enhance long-term survival and evolutionary fitness, Proc. Natl. Acad. Sci. USA **99**, 8737 (2002).

[30] E. R. Zinser, D. Schneider, M. Blot, and R. Kolter, Bacterial evolution through the selective loss of beneficial genes: Trade-offs in expression involving two loci, Genetics **164**, 1271 (2003).

[31] W. R. Shoemaker, S. E. Jones, M. E. Muscarella, M. G. Behringer, B. K. Lehmkuhl, and J. T. Lennon, Microbial population dynamics and evolutionary outcomes under extreme energy limitation, Proc. Natl. Acad. Sci. USA **118**, e2101691118 (2021).

[32] T. King, A. Ishihama, A. Kori, and T. Ferenci, A regulatory trade-off as a source of strain variation in the species escherichia coli, J. Bacteriol. **186**, 5614 (2004).

[33] M. Vulić and R. Kolter, Evolutionary cheating in escherichia coli stationary phase cultures, Genetics **158**, 519 (2001).

[34] A. J. Lee, S. Wang, H. R. Meredith, B. Zhuang, Z. Dai, and L. You, Robust, linear correlations between growth rates and β-lactam–mediated lysis rates, Proc. Natl. Acad. Sci. USA **115**, 4069 (2018).

[35] H. Beeftink, R. Van der Heijden, and J. Heijnen, Maintenance requirements: Energy supply from simultaneous endogenous respiration and substrate consumption, FEMS Microbiol. Ecol. **73**, 203 (1990).

[36] P. van Bodegom, Microbial maintenance: A critical review on its quantification, Microb. Ecol. **53**, 513 (2007).

[37] G. Wang and W. M. Post, A theoretical reassessment of microbial maintenance and implications for microbial ecology modeling, FEMS Microbiol. Ecol. **81**, 610 (2012).

[38] M. Lemonnier, B. R. Levin, T. Romeo, K. Garner, M.-R. Baquero, J. Mercante, E. Lemichez, F. Baquero, and J. Blázquez, The evolution of contact-dependent inhibition in non-growing populations of escherichia coli, Proc. R. Soc. B: Biol. Sci. **275**, 3 (2008).